Laser Chem., Vol. 13, pp. 63–83
Reprints available directly from the publisher
Photocopying permitted by license only

THE ROLE OF MOLECULAR COMPLEXES IN A HOLLOW-CATHODE CW $HeCd^+$ LASER

H. H. TELLE, C. GREY MORGAN, S. E. ACOSTA-ORTIZ[1] and KARYONO[2]

Department of Physics, University College Swansea, Singleton Park, Swansea SA2 8PP, United Kingdom

(Received 16 December 1992; in final form 19 January 1993)

The importance of molecular complexes in gas discharge lasers has long been recognised, and indeed they are the essence in excimer lasers. For other discharge lasers operating with gas mixtures, for example metal vapour lasers, the role of molecular complexes in the laser discharge has hardly been addressed. In this work the emission from a cw multi-colour hollow-cathode $HeCd^+$ laser has been investigated spectroscopically, and emphasis was placed on the detection of molecular bands. Specifically the presence of He_2^* in the laser discharge was confirmed which is thought to play a major role in the generation of the green laser lines. Emission bands attributed to the Cd_2^* metal dimer were identified; however, this dimer does not seem to be of importance in the laser process. In addition to the He_2^* and Cd_2^* emission strong molecular continuum bands, exhibiting gain, were observed which accompany all laser lines; these can only be interpreted as originating from transitions in the ionic complex $(He{\cdot\cdot}Cd^+)^*$.

1. INTRODUCTION

Hollow-cathode $HeCd^+$ lasers have been studied extensively since their first successful demonstration.[1] One of the major interests in this kind of laser is its attractive capability to oscillate simultaneously on a number of transitions, and in particular it can be adjusted to deliver "white" light, a balanced mixture of the primary colours blue (441.6 nm), green (533.7/537.8 nm) and red (635.5/636.0 nm). Since the first realization of white light emission[2] several laser configurations have been proposed and tested in order to improve the laser output characteristics (see e.g.,[3]). A commercial $HeCd^+$ white-light laser is now available. Despite the successful operation of $HeCd^+$ lasers there still remain open questions, in particular controversy persists over the population mechanisms of some of the upper laser levels.

It is widely accepted that the upper laser levels for the red lines (6g ^2G) and those for some infrared transitions (6f ^2F for the 723.7 nm and 728.4 nm lines, 9s ^2S for the

[1] Permanent address: Centro de Investigaciones en Optica, A.C., 37000 Leon, Gto., Mexico.
[2] Permanent address: Department of Physics, Faculty of Mathematics and Science, Gadjah Mada University, Yogyakarta 55281, Indonesia.

865.2 nm and 887.8 nm lines) are predominantly populated by near-resonant charge transfer according to

$$He^+ + Cd \rightarrow He + Cd^+*(6f\ ^2F,\ 6g\ ^2G,\ 9s\ ^2S) + \Delta E \quad (1)$$

The upper levels of the blue and UV lines are thought to be populated via Penning ionization or direct electron impact excitation, i.e.,

$$He^m(2s\ ^1S,\ ^3S) + Cd \rightarrow Cd^+*(5s^2\ ^2D) + He + e^- \quad (2)$$

and

$$e^- + Cd \rightarrow Cd^+*(5s^2\ ^2D) + 2\cdot e^- \quad (3)$$

Baltayan *et al.*[4] attribute 22% of the population to the Penning process and 78% to electron impact excitation, Grey Morgan *et al.*[5] quote 40% and 60%, respectively, and Boulmer-Leborgne *et al.*[6] give values of 25% and 75%. It should be mentioned that it also has been argued that metastable molecular helium, $He_2^m(^3\Pi_g,\ ^3\sum_u^+)$, may contribute to the population of $Cd^+(5s^2\ ^2D)$; for the lowest vibrational levels of He_2^m energetically this is just possible (see Figure 1).

The red laser lines terminate in the $4f\ ^2F$ levels which are the upper levels of the green laser lines; thus it was suggested tht they were populated via radiative cascading (see e.g.,[7]). However, this is inconsistent with the pressure dependence of the red and green lines; while the red lines disappear for higher pressures of helium the green lines continue to show strong laser action (see e.g.,[8]). Moreover, the threshold discharge current for the green lines was found to be lower than that for the red lines (see e.g.,[9]). A number of alternative excitation mechanisms was proposed, for example electron

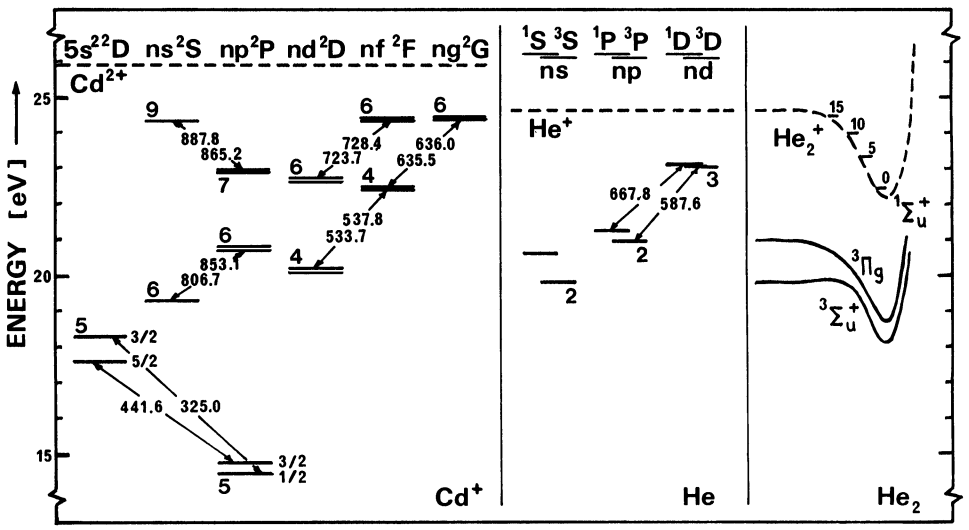

Figure 1 Partial energy level diagram for Cd^+, He, He_2 and He_2^+; the designation of levels is given at the top pf the diagram while the principle quantum number n is given next to the levels. Some of the relevant transition lines are given, together with their wavelengths (in nm).

recombination (see e.g.,[10]), direct electron impact (see e.g.,[11]), or charge transfer from the molecular ion He_2^+ (see e.g.,[12]). Only the latter process is likely to play a major role under the conditions of high pressure in the hollow-cathode laser tube. Furthermore, experimentally it has been shown[13] that the number density of He_2^+ increases at the expense of He^+ for high pressure in a helium discharge. Thus it is reasonable to assume that for low pressures the radiative cascade population process dominates, i.e.,

$$He^+ + Cd \rightarrow He + Cd^+*(6g\ ^2G) + \Delta E$$

$$Cd^+*(6g\ ^2G) \rightarrow Cd^+*(4f\ ^2F) + h\nu_{red}, \qquad (4)$$

and that for high pressures the nearly resonant charge transfer with He_2^+ in low vibrational levels dominates, i.e.,

$$He_2^+ + Cd \rightarrow 2\cdot He + Cd^+*(4f\ ^2F). \qquad (5)$$

Ranjbar *et al.*[14] speculated that He_2^+ also could be responsible for population of the $5s^2\ ^2D$ levels (upper levels for the blue and violet laser lines); however, they have assumed an incorrect potential energy well for He_2^+, between 18.2 eV and 20.2 eV, while the now accepted value is around 22 eV. Thus population of the ^2D levels via He_2^+ is rather unlikely.

A summary of the important energy levels and radiative transitions discussed above is given in Figure 1 (partial energy level diagram).

The processes of relevance for the different population mechanisms have been widely investigated using spectroscopic techniques, but usually in afterglow measurements or in discharge devices which do not lend themselves for laser action. It is not necessarily correct to assume that results from measurements under non-lasing conditions hold for a real laser.

It has been the aim of this investigation to perform a parametric spectroscopic study of a hollow-cathode HeCd$^+$ laser, for the first time, under operating conditions. Of central interest was to examine the presence of molecular species in the laser discharge and determine their importance for the lasing process, in particular for the green transitions.

2. EXPERIMENTAL SYSTEM

The HeCd$^+$ laser used in this investigation is based on a multi-segment hollow-cathode discharge tube, comprising 10 anodes and 9 cathodes with a total discharge length of 60 cm. The laser usually operates at total gas pressures in the range 3–50 mbar for discharge current typically in the range of 0.06–0.15 A per anode (total current 0.6–1.5 A). The cadmium vapour pressure can be adjusted in the range 0.003–0.3 mbar. The cavity of 160 cm length consists of two concave mirrors of 500 cm curvature; the mirrors have a broadband high-reflectivity coating ($R \geqslant 99.5\%$) allowing the laser to oscillate simultaneously on all known transitions in the visible as well as on the lines 723.7/728.4 nm. Details of the laser configuration are given elsewhere.[15,16]

A schematic diagram of the experimental arrangement is shown in figure 2. The light used for spectroscopic analysis is coupled out of the system via the Brewster

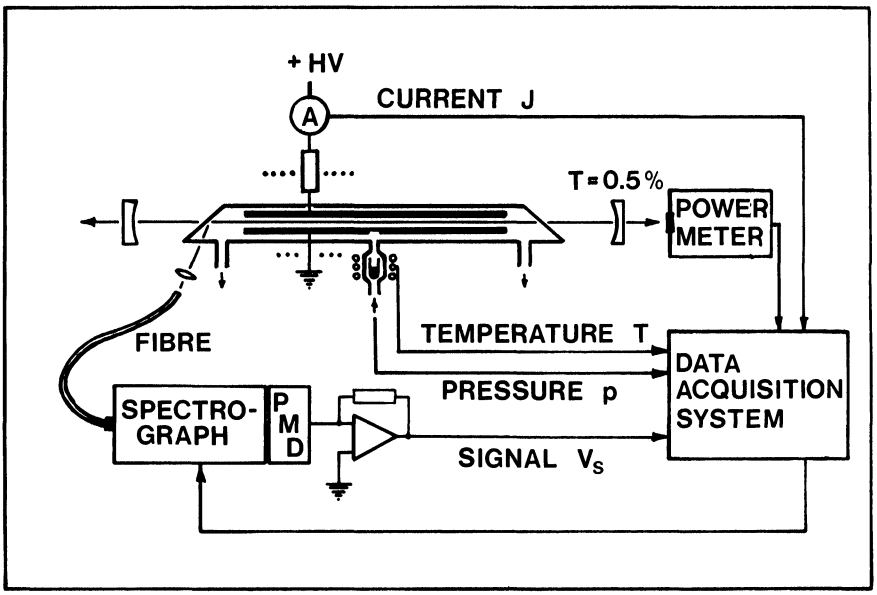

Figure 2 Experimental system for the spectroscopic investigation of the hollow-cathode laser; PMD = photomultiplier or photodiode.

windows of the discharge tube. Although this arrangement strongly reduces the amount of radiation being collected from the discharge to just a few percent of the maximum possible if one were looking directly into the discharge, it allows spectral analysis while the laser oscillates. To our knowledge this is the first such systematic, spectroscopic study under lasing conditions, and this is of crucial importance for the understanding of laser action, as will be discussed later.

The collected light is directed via a large-core quartz fibre into a monochromator; its resolution is adjustable but is typically set for a linewidth of $\Delta\lambda \simeq 0.5$ nm which is sufficient to resolve most spectral features but at the same time allows ample intensity through the system for sensitive detection with good signal-to-noise ratio. The dispersed light is collected via a photodiode—amplifier or a photomultiplier—amplifier combination. In the blue/green part of the spectrum the latter has a total amplification superior by a factor of approximately 30, but in the red and more so near-infrared it drops significantly below that of the photodiode system. Data sampling, averaging, storage and analysis is performed by a computer-controlled boxcar integrator system.

Spectra were recorded in the region 300–850 nm which covers most of the known laser transitions observed in hollow-cathode $HeCd^+$ lasers; the recordings were made for both lasing and non-lasing conditions. The latter condition means that all discharge conditions were kept constant while either one mirror was blocked or alternatively, tilted until lasing ceased. This procedure allows systematic study of line intensities, as a function of the various discharge parameters, and avoids misinterpretation of intensity changes. Besides the strong laser transitions most of the tabulated lines of the neutrals He and Cd were observed as well as numerous lines of the ions He^+

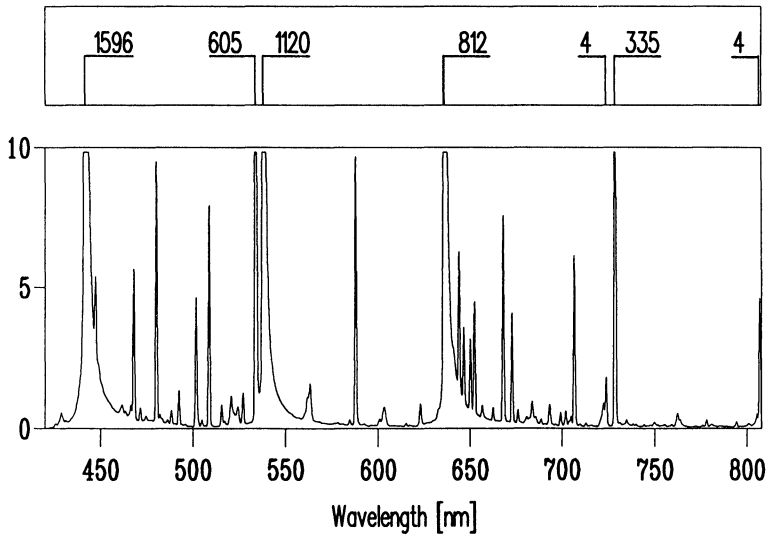

Figure 3 Overview laser spectrum. The laser lines are out of scale and their amplitudes are given at the top of the figure; the 723.7 nm and 806.7 nm lines are not oscillating under the experimental conditions for this recording.

and Cd^+; in addition the spectra revealed molecular features. In this paper emphasis will be placed on these molecular contributions; a discussion of the full parametric study of the laser transitions will be given in a forthcoming publication.[17]

An example of a laser emission spectrum is shown in Figure 3. The scale of the display has been chosen so that (weak) molecular bands should be recognized; of course, the laser lines are saturated on this scale. In the figure strong asymmetric broadening of the laser lines is observed. This was rather surprising since basically weak emission bands from He_2 and Cd_2 dimers were expected. However, on second thoughts, the observation is not unexpected since spectral broadening of metal atom—rare gas atom complexes is a well known and a frequently observed phenomenon in systems with particle densities similar to those in this $HeCd^+$ laser discharge.

In the following sections we describe the molecular features observed in our spectroscopic investigation, i.e., those of the dimers He_2, Cd_2 and the $He{\cdot\cdot}Cd^+$ complexes, and discuss their origin and their role in the lasing processes. Most of the discussion will be based on data in the blue/green range of the spectrum since there the highest sensitivity and best signal-to-noise ratio could be achieved with the available equipment.

3. EMISSION BANDS OF He_2^*

3.1. The Formation of He_2^+

When helium atoms in their ground state, $He(1s^2\ ^1S_0)$, collide with energetic electrons, e^-_{fast}, excitation into high-lying electronic states or ionization occurs. In the case of

increasing atom number density, secondary processes lead to the formation of molecular species, namely the molecular ion $He_2^+(X\ ^2\Sigma^+)$ which is rather strongly bound with a potential well of over 2 eV. The molecular ion is created via two major mechanisms, i.e., associative ionization (known as the *Hornbeck-Molnar process*) or three-body collisions (known as the *Holt-Biondi process*).

The Hornbeck-Molnar process can be thought of as a collision sequence according to

$$\begin{aligned} He + e^-_{fast} &\rightarrow He^{**} + e^- + \Delta E \\ He^{**} + He &\rightarrow He_2^+(X,v'') + e^- + \Delta E \end{aligned} \qquad (6)$$

in which the second collision has to occur within less than $\simeq 10^{-7}$ s after the excitation of He** (the lifetimes of the excited states). The appearance potential for the process was established for electrons with kinetic energy of $22.5\,eV < e^-_{fast} < 24.2\,eV$ (see e.g.,[18]). Accordingly He** is created in an excited state ($n\ ^{2s+1}L$), with $n \geqslant 3$ (see e.g.,[19]). The rate of production of He_2^+ is of the order of 10^{14}–$10^{15}\,cm^{-3}\cdot sec^{-1}$ and is increasing for higher-lying states.

In addition to the associative ionization process described by equation (6) it was found[20] that molecular ions may also be formed by energy-pooling collisions between helium atoms in their metastable states, predominantly $He^m(2s\ ^3S_1)$, according to

$$He^m + He^m \rightarrow He_2^+ + e^- + \Delta E. \qquad (7)$$

For increasing pressure associative formation of molecular ions is dominating over the formation of atomic ions because the ionization potential of He_2^+ is lower than that of He^+ by the value of the binding energy of the molecular ion of $\simeq 2.16$ eV.

The Holt-Biondi process, first proposed in 1950,[21] can be thought of as a collision sequence according to

$$\begin{aligned} He + e^-_{fast} &\rightarrow He^+ + 2\cdot e^- + \Delta E \\ He^+ + 2\cdot He &\rightarrow He_2^+(X,v'') + He + \Delta E \end{aligned} \qquad (8)$$

in which the second part, the three-body collision process, is only observed at higher pressures.

The presence of molecular ions, He_2^+, has been confirmed in mass spectrometric investigations (see e.g.,[22]) of electron impact excitation in discharges of a few mbar of helium. However, it is usually impractical or impossible to mass-detect He_2^+ in a laser discharge tube; thus indirect detection methods are necessary. The products of collisional radiative recombination readily lend themselves for this purpose: a number of reasonably strong molecular emission bands of He_2^* can usually be observed in helium discharge spectra.

3.2. *The Formation of He_2^**

The generation of molecular emission bands may be described in general form by the sequence

$$\begin{aligned} He_2^+ + e^- + A &\rightarrow He_2^{**} + A + \Delta E \\ He_2^{**} &\rightarrow He_2^* + h\nu_{band} \end{aligned} \qquad (9)$$

in which A may be any collision partner available in the discharge. Recombination processes according to equation (9) have been investigated quantitatively,[23] and it

has been established that generation of excited He_2^{**} is most likely when A is a further electron, e^-. It should be noted that in competition to process (9) dissociative recombination is observed which gives rise to atomic emission lines, i.e.,

$$\begin{aligned} He_2^+ + e^- &\rightarrow He^{**} + He + \Delta E \\ He^{**} &\rightarrow He^* + h\nu. \end{aligned} \tag{10}$$

For example, recombination into the 4d ^3D and 3d ^3D levels is evident from the persistent emission to the 2p ^3P levels at 447.2 nm and 587.6 nm, respectively, while other atomic transitions are heavily quenched at the required high pressures for molecular formation (see e.g.,[24]). This has been confirmed by data obtained in the present study.

Numerous molecular emission bands of He_2 have been observed and assigned, and a considerable number of them has been discussed by, among others, Collins and Robertson[13] who studied He flowing afterglow emission for a wide range of pressures. Bands at around 368 nm ($4p\ ^3\Pi_g \rightarrow 2s\ ^3\Sigma_u^+$), 398 nm ($5d\ ^3\Pi_u \rightarrow 2p\ ^3\Pi_g$), 445 nm ($4d\ ^3\Sigma_u^+ \rightarrow 2p\ ^3\Pi_g$), 465 nm ($3p\ ^3\Pi_g \rightarrow 2s\ ^3\Sigma_u^+$), 513 nm ($3p\ ^1\Pi_g \rightarrow 2s\ ^1\Sigma_u^+$), 587 nm ($3d\ ^3\Pi_u \rightarrow 2p\ ^3\Pi_g$) and 595 nm ($3d\ ^3\Sigma_u^+ \rightarrow 2p\ ^3\Pi_g$) were observed, together with further unassigned structures around 610 nm, 630 nm and 640 nm. The vibrational (0-0) transitions were usually found to be the strongest while other vibrational transitions were rarely noticeable but for traces of some isolated strong rotational lines. For some bands it was found that their emission intensity followed the concentration of He_2^+, indicating that He_2^* was generated by radiative recombination from the molecular ion; this has been shown, for example, for the 465 nm band.[13]

3.3. *He_2^* Bands Observed in the Laser Discharge*

The observation and assignment of emission bands in He_2^* is in general rather difficult. Firstly, the probability of the formation of rare gas dimers is relatively low, and thus the overall intensity of a particular transition is weak. Secondly, many of the He_2^* states are strongly bound, by as much as 2.5 eV, although the He_2 ground state only forms a weakly bound van der Waals complex. As a consequence of the low mass of the molecule the vibrational and rotational states are widely spaced, and transitions between them are often scattered across a broad range of wavelengths reducing spectral density of a transition of already weak intensity even further.

In our segmented hollow-cathode discharge laser tube molecular band emission of He_2^* at 445 nm, 465 nm, 595 nm, 610 nm, 630 nm and 640 nm could clearly be identified and has been studied parametrically for a range of pressures and discharge currents.[16,25] The relative intensity of He_2^* bands was strongly dependent on helium pressure and over the investigated range increased by at least a factor of two. However, no attempt was made to fully quantify the contribution from individual bands since they often strongly overlap each other (our spectral resolution was insufficient to resolve the rotational structure) and simultaneously their shape changes significantly due to varying population distributions in the vibrational-rotational manifold.

A representative sample of spectra exhibiting He_2^* emission bands is shown in Figure 4. For the sake of clarity the displayed spectra were recorded for a discharge in helium (the cadmium reservoir was not heated) but under the same conditions as for the helium/cadmium mixture used for laser operation; the atomic and molecular helium features in the laser mixture are basically identical but superimposed a number

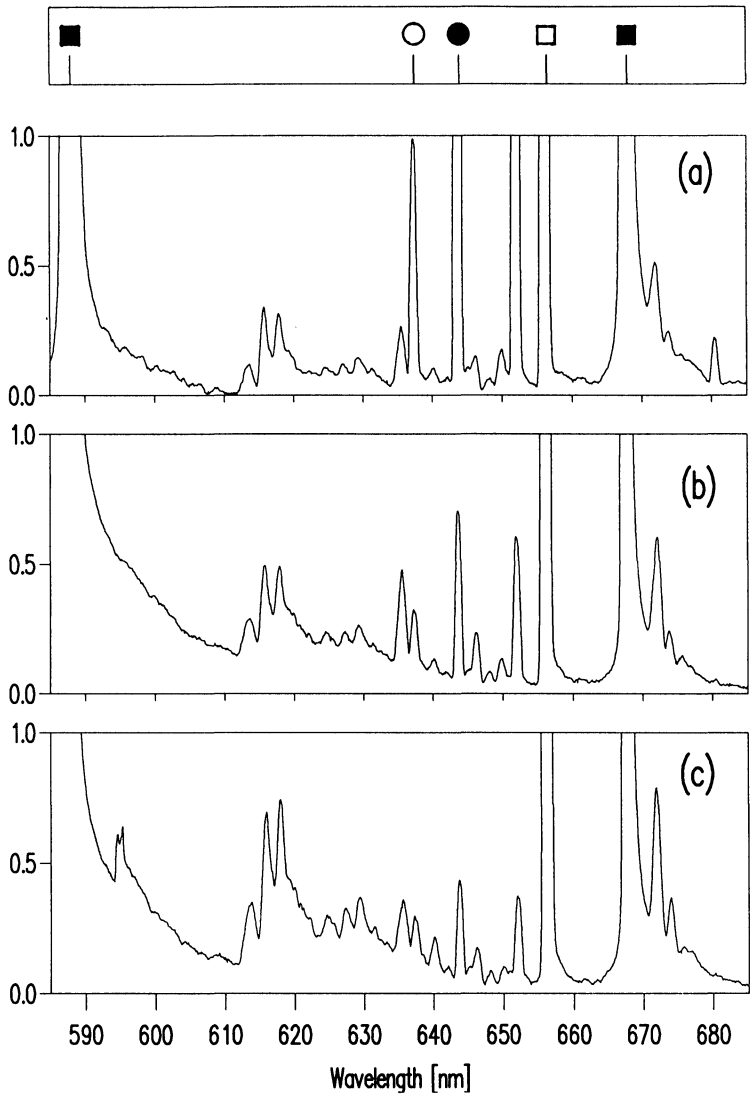

Figure 4 Helium discharge spectra from the laser tube at (a) 5 mbar, (b) 20 mbar and (c) 40 mbar He pressure (cadmium reservoir not heated). The spectra are scaled to reveal molecular features. Major atomic and ionic transition lines are indicated at the top of the figure (■ He, □ He^+, ● Cd, ○ Cd^+), and their pressure dependence is given in Figure 5.

of cadmium lines. It is clearly seen that the molecular features increase when the pressure rises, at the expense of the atomic transitions. This is graphically illustrated in Figure 5 in which the relative change in intensity is plotted as a function of pressure. Two strong atomic lines have been selcted, the $2p\ ^3P^0 \rightarrow 3d\ ^3D$ transition at 587.6 nm and the $2p\ ^1P^0 \rightarrow 3d\ ^1D$ transition at 667.8 nm; these are compared with two molecular features at 618 nm and at 630 nm which are reasonably representative for the molecular

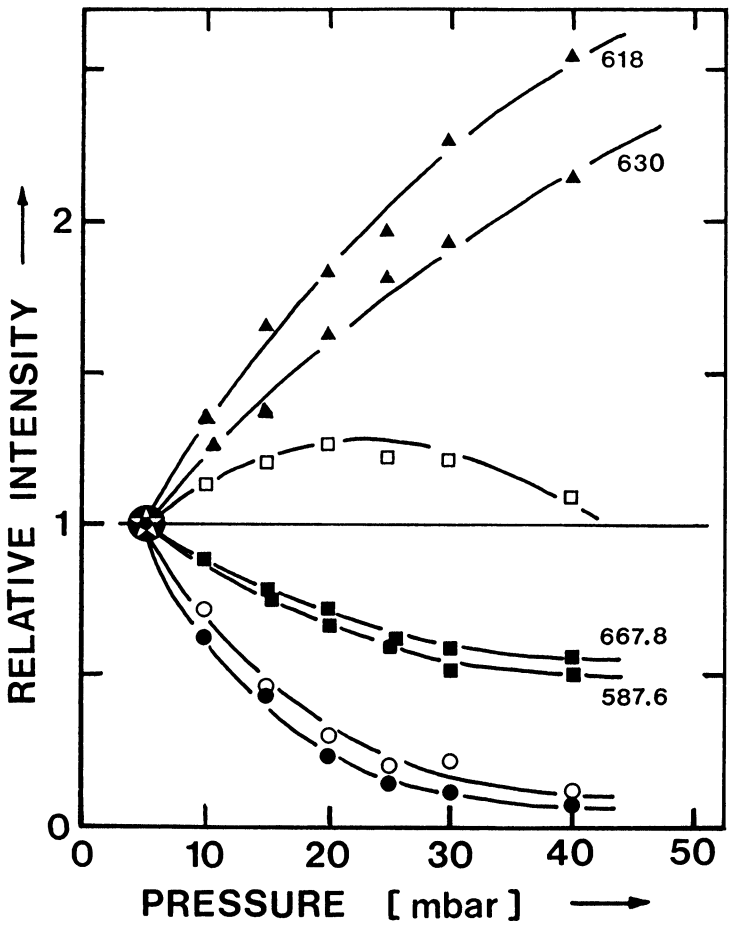

Figure 5 Pressure dependence of selected atomic and ionic lines, and He_2 features, as shown in Figure 4 (■ He, □ He^+, ▲ He_2, ● Cd, ○ Cd^+); all data are normalized to unity at 5 mbar.

emission in the spectral region 610–640 nm. The relative emission intensity has been normalized to the one at 5 mbar.

Besides the banded structure shown in Figure 4 and that observed in other spectral regions excimer-type continuum emission accompanies all atomic lines, most notable the strong lines (see e.g., the 587.6 nm and 667.8 nm lines). Throughout the spectral range we investigated (300–850 nm) the shading of the line satellite is towards longer wavelengths. These features may be attributed to transitions from a (bound) molecular upper state to the repulsive part of the potential of a lower state; this is a well known characteristic for numerous excimer transitions. It should be noted that the molecular continuum emission increases in intensity and changes its shape while the atomic emission at the centre of the feature decreases; this is consistent with the findings described in the previous paragraph.

We would like to point out that excimer bands between excited states of the He_2

or the other rare-gas dimers have not previously been reported. On the other hand, the existence of continuum bands is well known for transitions from the lowest-lying molecular resonance states to the ground state of the dimer; such a transition is exploited in the Xe_2 excimer laser.

4. EMISSION BANDS OF Cd_2^*

4.1. The Formation of Metal Dimers

When the particle density in metal vapours is increased a strong tendency is found for the formation of aggregates and in particular dimers. There are similarities but also distinct differences for metal dimer formation, in particular for the group 1 and group 2 elements.

As a general rule group 1 metal dimers exhibit a rather strongly bound ground state potential with a well depth of usually around 0.5 eV. This is due to the fact tht the single valence electrons of the two separate atoms give rise to a strong paired-off bond. Some of the excited states may be bound even more strongly with well depths of up to 1 eV, or more. As a consequence, transitions from low vibrational levels in such an excited state will be at wavelengths much longer than the transitions in the atomic correlation products, and the related vibrational sequence may extend over tens of nanometers. This phenomenon has been investigated most extensively for the sodium dimer, Na_2 (see e.g.,[26]). It has also been exploited to generate laser action in optically excited Na_2^* which is well documented (see e.g.,[27]).

The situation is rather different for the group 2 metals. For these elements the valence shell, ns^2, is filled and thus their behaviour is similar to that of the rare gases, i.e., the ground state exhibits only a shallow van der Waals minimum of usually less than 0.1 eV. On the other hand, some of their excited states can be strongly bound, up to 0.5 eV, because the symmetry of a closed shell is broken. Although the group 2 dimers have been investigated less frequently than the group 1 dimers there are some data available for the alkaline earth (group 2a) dimers (see e.g.,[28]). However, rather little is known about the spectroscopy of group 2b dimers; Cd_2 belongs to this group.

The potential minimum of the lowest bound excited dimer states is often at a shorter interatomic separation than the ground state minimum; thus transitions from an upper bound state often terminate at the repulsive part of the ground state potential giving rise to continuum emission which may extend over many nanometers. The phenomenon is well known and is exploited in excimer lasers.

A few years ago it was speculated that mixed metal excimer molecules could become candidates for short-wavelength lasers which could be excited by electron bombardment, and in particular mixtures of mercury and cadmium were considered (see e.g.,[29]). However, laser action was not achieved and it was argued that absorption in Cd_2 could be the cause that no gain was obtained. Despite the discussion about the role of the Cd_2 dimer its spectroscopy was hardly pursued, and only very few investigations have been performed in recent years.[30,31]

4.2. Cd_2^* Emission Observed in the Laser Discharge

In Figure 6 a comparison is given between a spectrum of a discharge in pure helium (Figure 6a) and a mixture of helium and cadmium (Figure 6b). For the recording of

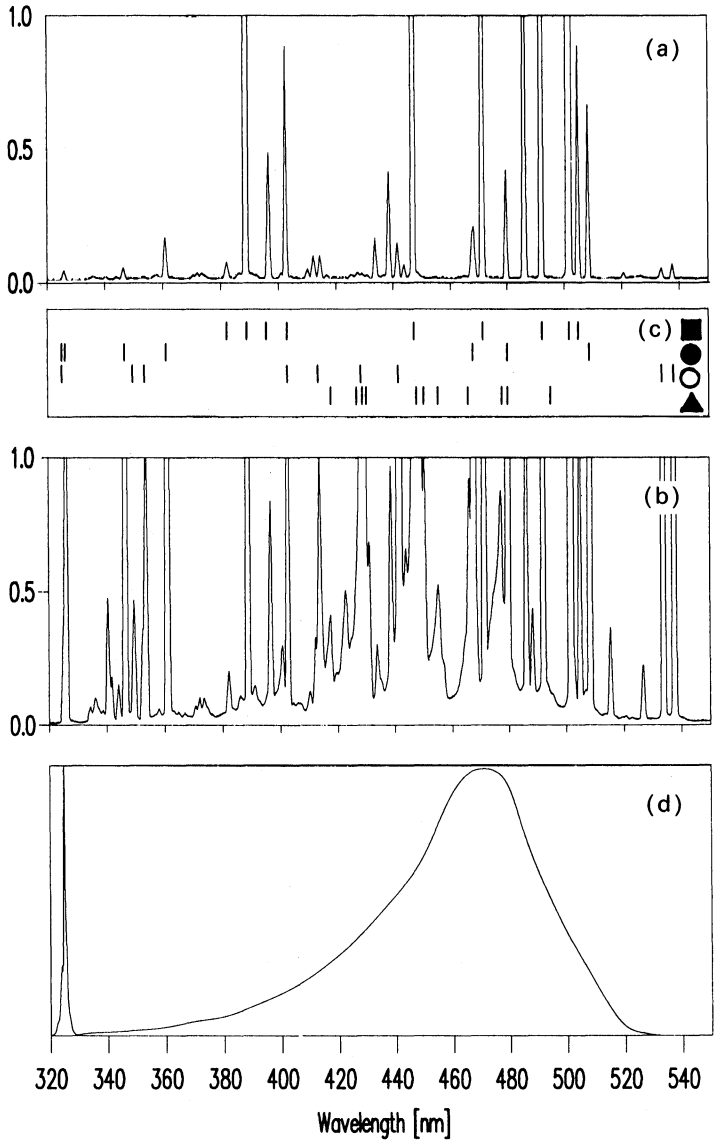

Figure 6 Spectral emission attributed to Cd_2^*; (a) discharge in helium at 5.1 mbar, (b) discharge in a mixture of helium at 5.25 mbar and cadmium at 0.07 mbar partial pressure. Atomic and ionic lines (■ He, ● Cd, ○ Cd^+) and some unidentified band features (▲) attributed to Cd_2^* are marked in (c); for details see text. For comparison blue and red wings to the Cd 325 nm line, after[30] and[31], are shown in (d); their scale is arbitrary.

the second spectrum the partial pressure of cadmium was adjusted to a rather high value (0.07 mbar) to ensure sufficient probability of dimer formation. One of the laser mirrors was blocked while the spectra were recorded to prevent oscillation; this was

due to avoid saturation of the detection system in the spectral region in which Cd_2^* emission was expected.

As can be seen a broad feature appears in the spectrum when cadmium is present in the discharge; this stretches from below 340 nm to beyond 520 nm, with maximum intensity around 470 nm (note that the spectra are not corrected for the response of the detection system which varies by approximately 20% over the range shown). The envelop of this structure is rather similar to the Cd_2^* emission spectrum published by Drullinger and Stock;[32] this is reproduced in Figure 6d. Their spectrum peaks around 470 nm and exhibits some undulations on the short-wavelength side of that maximum. The emission band is thought to be due to the transition $1_u \rightarrow 0_g^+$ (for a discussion see the next section).

Closer inspection of the spectrum in Figure 6b reveals a sequence of band-like features, shaded towards short wavelengths, which bears a striking resemblance to a vibrational progression.

4.3. Possible Origin of the Cd_2^* Emission

In order to trace the origin of molecular emission and to explain the shape of observed spectra knowledge of the molecular potentials is essential. Using basic selection rules one is also able to predict which states are connected via radiative transitions and roughly what intensity distribution is expected.

The ground state of the group 2a and 2b metals, M, is a $^1S_0$ state. Thus, according to correlation rules, the related dimer ground state, M_2,—made up from two ground state atoms $M(^1S_0)$—is a 0_g^+ (or $^1\Sigma_g^+$) state, where the *g* stands for *gerade* state (the notation in brackets is according to Hund's case *a*). For most of these metals the lowest excited state is a ^3P_J state with J = 0,1,2. Although triplet-to-singlet transitions are forbidden in pure LS-coupling and for pure dipole transitions the partial breakdown of these approximations allows one to observe the transition $^3P_1 \leftrightarrow {}^1S_0$ with reasonable intensity for most of the group 2 metals. Consequently, the lowest excited state potentials of the dimers for which allowed radiative transitions are expected will correlate to the pair $M(^1S_0) + M^*(^3P_1)$. According to the parity selection rule for homonuclear molecules allowed dipole transitions only connect *gerade* states, indexed *g*, with *ungerade* states, indexed *u*; thus only two excited state potentials have to be considered for transitions connected radiatively to the ground state potential, namely the 0_u^+ (or $^3\Pi_u$) and the 1_u (or $^3\Sigma_u^+$) potentials. As a rule-of-thumb the latter state is usually more strongly bound and lies energetically below the former state. This is schematically indicated in Figure 7. Note also that usually the (van der Waals) minima of the $\Omega = 0$ states are at larger interatomic separation than the minima for the $\Omega = 1$ states. A full theoretical description of the cadmium dimer potential manifold is given.[32]

The potential minima of the two $\Omega = 0$ states for Cd_2 are roughly at the same interatomic distance ($\simeq$4.5–5.5Å); the ground state is slightly stronger bound. Hence one expects a vibrational sequence over a narrow wavelength range on the low-wavelength side of the $Cd(^3P_1 \rightarrow {}^1S_0)$ line at $\lambda = 326.1$ nm; this has been confirmed experimentally.[31] Since the potential minimum of the $\Omega = 1$ state is at rather short interatomic separation ($\simeq$3.1Å) transitions from this state are to the repulsive part of the ground state potential, and hence give rise to continuum emission. The vibrational wavefunction of the upper state in such a transition is mirrored in the spectral intensity distribution. A summation over all vibrational levels has been

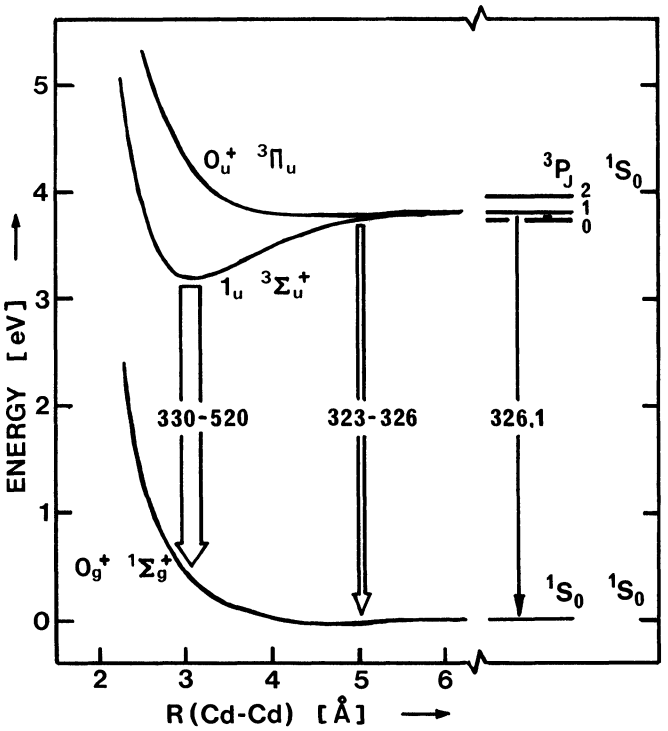

Figure 7 Relevant potential energy curves for the Cd_2 dimer, and possible emission lines and bands; potential energy data according to[32].

performed in[32] to generate a synthetic spectrum which exhibits the same shape and structure as the experimental spectrum (see[31] and Figure 6d) although the intensity maximum is generated at a lower wavelength than that found experimentally.

The additional band structure in Figure 6b, its position marked in Figure 6c, is though to have its origin not in the two transitions discussed above. The spacing of the features suggests that the related transition is between two bound states with relatively deep potential wells.

It has been found that there are some similarities between the spectral features in Cd_2 and Hg_2; this is not surprising since they are both members of the group 2b elements. Indications of the possible origin of banded structure in the case of Hg_2 are recorded in the literature; in their concise theoretical treatment Mies *et al.*[34] calculated a number of Hg_2 dimer potentials correlating to higher excitation states, and in particular a $1_u(2^1\Pi_u)$ state with a deep well is shown correlating to the $^3P + {}^3P$ asymptotes (see Figure 5).[34] Transitions from such a state to the somewhat shallower potentials of the 1_g or 0_g^+ states, correlating to the asymptotes $^3P + {}^1S$, would give rise to vibrational sequences similar to those observed in our spectrum (Figure 6b).

Bender *et al.*[33] in their theoretical investigation of Cd_2 briefly mention that they calculated some high-lying potentials, in analogy to the Hg_2 case. They indicate the possibility of a strong transition between the $^3\Pi_u$ state of the $Cd(^3P) + Cd(^3P)$ manifold

and the $^3\Pi_g$ state of the $Cd(^3P)+Cd(^1S)$ manifold, and estimate its wavelength to be around 403 nm. However, no further details are given.

On the other hand, the unassigned bands we observe are rather strong and their spacing is not typical for known transitions in metal dimers; one thus may suspect that they originate from a molecule other than Cd_2. However, no apparent match could be found to known emission bands of other molecules which could be present as a contaminant in the cadmium reservoir (the features only appear when cadmium is admitted into the discharge).

At this stage of the investigation we have made no further effort to trace the exact origin of all observed bands thought to belong to Cd_2^* emission for the lack of molecular potentials and insufficient experimental data. Further experimental and theoretical investigations are planned for the future, in particular experiments with increased spectral resolution.

5. EMISSION BANDS OF THE COMPLEX $(He{\cdot\cdot}Cd^+)^*$

5.1. The Formation of Complexes between Metal and Rare-gas Atoms

Collisional processes are responsible for the observation of far wings in atomic lines, i.e., deviations from simple Lorentzian functional form (primarily related to the natural linewidth) or Gaussian functional form (related to Doppler broadening). The line profile in the presence of an atomic, or molecular, pertuber is closely related to the interaction potentials between the atoms at short interatomic distances.

The far wings of the resonance lines of alkali atoms perturbed by rare-gas atoms in their ground state have been investigated extensively, both theoretically and experimentally (see e.g.,[35]). For a substantial number of transitions in a variety of rare-gas—neutral-alkali-metal complexes agreement between theoretical calculations and experimental values becomes increasingly improved.

In comparison, data on collisional broadening of metal-ion spectral lines by rare gases are scarce although e.g., Mg^+ and Ca^+ resonance lines are of great interest in astrophysics: they exhibit some peculiar features in solar and stellar spectra which are of increasing importance in the modelling of stellar atmospheres. Nearly no information is available for other rare-gas—metal-ion complexes. One of the few examples is the recently conducted theoretical study of $Ne{\cdot\cdot}Al^+$ and $Ar{\cdot\cdot}Al^+$;[36] subsequently to the theoretical investigation a broad emission band of the $(Ar{\cdot\cdot}Al^+)^*$ excimer near 193 nm was observed.[37] Neither theoretical nor experimental data are found in the literature for the $He{\cdot\cdot}Cd^+$ pair.

5.2. $(He{\cdot\cdot}Cd^+)^*$ Emission Observed in the Laser Discharge

It has been pointed out in section 2 where the general experimental procedure is described that all laser lines exhibit very strong asymmetry. In the overview spectrum (Figure 3) this can be seen for the blue, green and red laser transitions. The same is also observed when the laser is adjusted to oscillate on the IR transitions as well (see reference[9]). These features appear and disappear together with laser action. The wings of the laser lines extend over a wide wavelength range which is much broader and very different in shape from a Lorentzian or Gaussian wing. We thus conclude that

these features can not be attributed to the transitions in the metal ion which are generally accepted to be responsible for the observed laser emission.

In order to establish the origin of the line asymmetry a parametric study has been undertaken, along the same principles which are usually followed to determine the dependence of laser action in discharge lasers on parameters such as total and partial pressures, discharge current, etc. A selection of spectra recorded for a set of different total pressures is displayed in Figure 8, covering the wavelength range of the blue and green laser transitions. In this paper the discussion is restricted to these laser

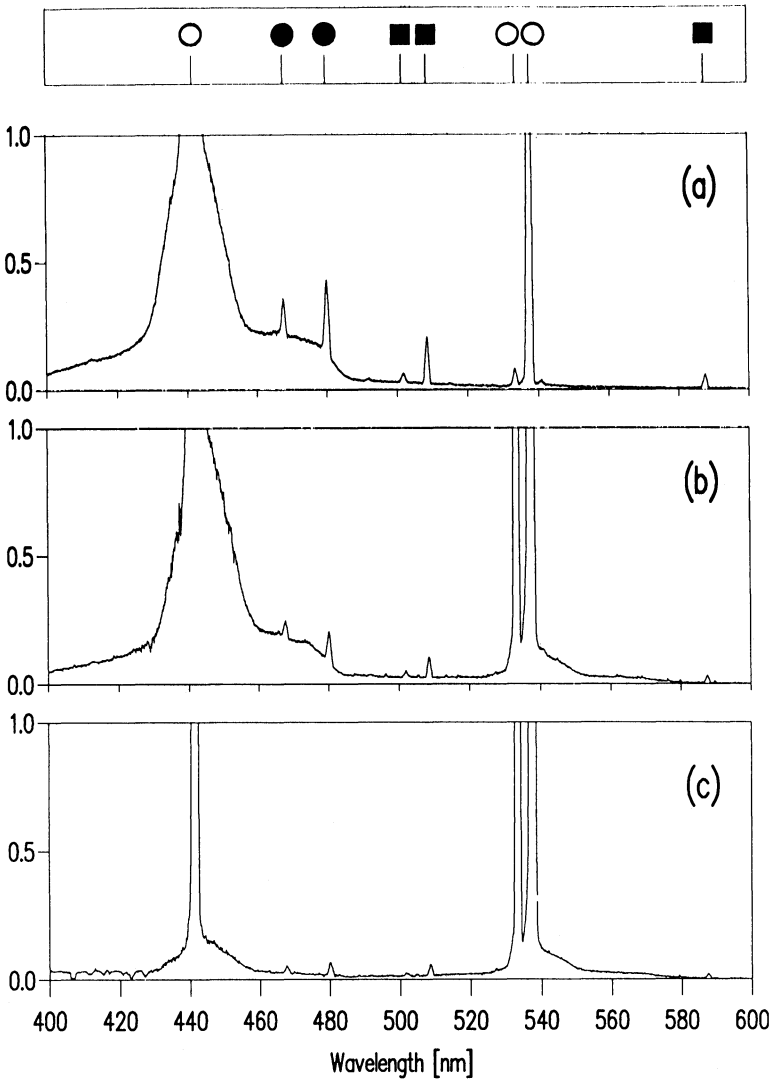

Figure 8 Molecular laser features for (a) 5 mbar, (b) 15 mbar and (c) 25 mbar total pressure; selected atomic lines are marked at the top of the figure (■ He, ● Cd). Related intensity data are collected in Table 2.

Table 1 Operational parameters for the $HeCd^+$ laser

He pressure	3–50 mbar
He flow rate	1 l/min
Cd reservoir temperature	336°C
Cd vapour pressure	0.18 mbar
Discharge current	1.3 A

lines because (i) the light detection system was most sensitive in this region, (ii) the mirror coating had much higher losses for the red and IR laser transitions which thus were much more susceptible to small variations in the discharge conditions, and (iii) the range of pressures for which laser action is achieved for the red and IR lines is rather narrow ($\simeq$3–12 mbar). Besides the variation of the total pressure all other parameters for the spectra in Figure 8 are constant; these are collected in Table 1.

As can be seen the asymmetric wing follows in its intensity behaviour that of the central transition in the Cd^+ ion (see Figure 8 and Table 2). For the blue laser transition the wing is observed in the range from 2 mbar to 27 mbar and for the green laser transition in the range from 5 mbar to beyond 50 mbar; these are also the ranges over which lasing for the individual transitions can be achieved. In addition to variations in intensity it is also observed that the shape of the wings changes.

Following the arguments for the origin of wings the observed emission is attributed to transitions in the complex $(He{\cdot\cdot}Cd^+)^*$; further details will be discussed in the following section. From the appearance of the wing intensity it seems that the molecular feature exhibits gain. This is quite strikingly illustrated in Figure 9 in which for the upper trace one of the mirrors has been blocked to suppress laser action. While the helium lines in the displayed spectral range are nearly unaltered the laser line and its wing drop dramatically, as expected. On the expanded scale (times 20) molecular features of rather similar shape can still be observed.

When inspecting the wings of the laser lines it is rather suggestive that they originate from at least two different molecular transitions.

One band extends over an extremely large range of tens of nanometers. For the blue laser line (441.6 nm) this broad blue wing extends to below 400 nm and the red

Table 2 Intensity ratio of atomic and molecular features of the blue and green laser transitions (data according to Figure 8 and other related spectra). The integrated molecular intensity is given as a percentage of the atom line intensity; —nl— = not lasing

Pressure mbar	I_{441} mW	$\int I_{mol}$ %	I_{533} mW	I_{537} mW	$\int I_{mol}$ %
3	1.2	11.5	—nl—	—nl—	—
5	2.7	19.8	—nl—	0.4	3.2
15	1.5	20.1	0.4	1.3	7.1
25	0.3	8.3	0.7	1.7	8.2
27	—nl—	—	0.8	1.8	8.7

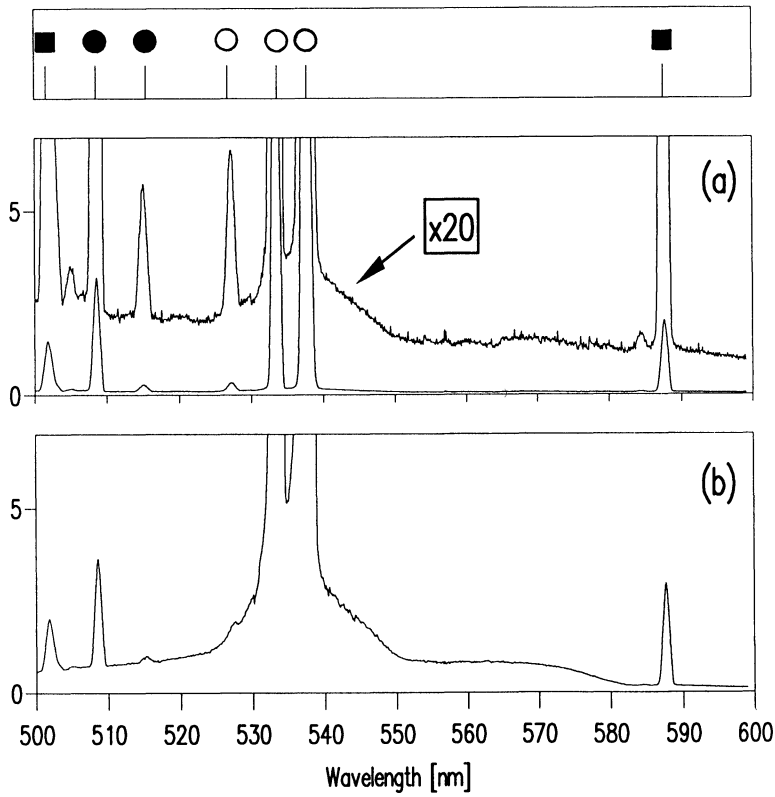

Figure 9 Molecular laser features for 15 mbar total pressure. Spectra were recorded (a) for one mirror blocked (non-lasing condition), and (b) while the laser was oscillating. On the × 20 scale in (a) molecular bands similar to those in (b) can be identified; selected atomic and ionic lines are marked at the top of the figure (■ He, ● Cd, ○ Cd^+).

wing to ≃485 nm where it exhibits a sharp drop, similar to a satellite. For the green laser lines (533.7/537.8 nm) this feature stretches between ≃500 nm and ≃580 nm; the observed long-wavelength satellite edge is usually not as pronounced as for the blue laser line but is clearly developed for a number of combinations of operating parameters not shown in this paper.

A second much narrower wing structure is observed on top of the broad feature, extending 3–8 nm on either side of the central laser line.

5.3. *Possible Origins of the* $(He{\cdot\cdot}Cd^+)^*$ *Emission*

In principle it is not surprising that more than one individual molecular transition is observed since the formation of the suspected $(He{\cdot\cdot}Cd^+)^*$ complexes involves atoms in S, P, D and F states. According to molecular correlation recipes their involvement will give rise to a manifold of molecular states characterised by their total angular momentum $\Omega = 0$, 1, 2 and 3 (or in Hund's case *a* notation $\sum$, Π, Δ and Φ states).

Table 3 Correlation between atomic and molecular states relevant in the formation of $(He\cdot\cdot Cd^+)^*$

Atomic asymptote $Cd^+ + He(^1S_0)$	Molecular state (Hund's case *a*)
$^2S_{\frac{1}{2}}$	$^2\Sigma^+_{\frac{1}{2}}$
$^2P_{\frac{1}{2}}$	$^2\Pi_{\frac{1}{2}}$
$^2P_{\frac{3}{2}}$	$^2\Sigma^+_{\frac{1}{2}}$, $^2\Pi_{\frac{3}{2}}$
$^2D_{\frac{3}{2}}$	$^2\Pi_{\frac{1}{2}}$, $^2\Delta_{\frac{3}{2}}$
$^2D_{\frac{5}{2}}$	$^2\Sigma^+_{\frac{1}{2}}$, $^2\Pi_{\frac{3}{2}}$, $^2\Delta_{\frac{5}{2}}$

The asymptotic correlation between the atomic and molecular states relevant to the $HeCd^+$ laser is given in Table 3. Applying the selection rules for electric dipole radiation a number of transitions between the individual manifolds is possible in principle although their relative strength is usually not known *a priori.*

As has been pointed out in section 5.1 to our knowledge no theoretical calculations for the $Cd^+ - He$ pair are reported in the literature thus no potential energy curves were available to deduce possible spectral emission bands.

However, we may draw some conclusions in analogy to the complexes between group 2 ions and rare gas atoms. Closest to the $Cd^+ - He$ systems are the Ca^+, $Sr^+ - He$ pairs for which some theoretical calculations have been performed.[38,39] Their theoretical treatment follows the convenient approach of employing the pseudo-potential model (see e.g.,[40]), exploiting the fact that singly ionized group 2 elements have the isoelectronic structure of neutral group 1 metals; the model has been applied to the latter systems with great success. Because of the complexity of modeling interaction potentials involving atoms in high annular momentum states it is not surprising that usually potentials have been calculated which converge asymptotically to S and P states, although also D states have been considered for a number of systems. No information on higher angular momentum states has been published to our knowledge.

In the light of the available data we have only tried to draw some schematic potential energy curves which may be involved in the generation of the observed wings to the blue laser line. For that transition only a subset of potentials has to be considered, correlating to the $^2D_{5/2}$ and $^2P_{3/2}$ asymptotes. These potentials are schematically shown in Figure 10.

The energetic order of the potentials is thought most likely to be correct; for example, as a general rule for potentials correlating to the same atomic asymptote Π-states are lower in energy than Σ-states, and the latter are often repulsive but for a possible shallow van der Waals minimum at large interatomic separation. The energy spacing in the $Cd^+ + He$ asymptote is correct while the well depths of the potentials are only qualitative although the indicated depths of 0.1–0.2 eV are typical for a number of metal atom—rare gas pairs.

The selection rules for electric dipole transitions for Hund's case *a* are $\Delta\Lambda = 0, \pm 1$ and $\Delta\Sigma = 0$; the related transitions are drawn in full arrows in Figure 10. The transitions $^2\Sigma^+_{1/2} \rightarrow {}^2\Sigma^+_{1/2}$ and $^2\Sigma^+_{1/2} \rightarrow {}^2\Pi_{3/2}$ will generate wavelengths rather close to the central atomic line while the $^2\Delta_{5/2} \rightarrow {}^2\Pi_{3/2}$ and $^2\Pi_{3/2} \rightarrow {}^2\Pi_{3/2}$ transitions are

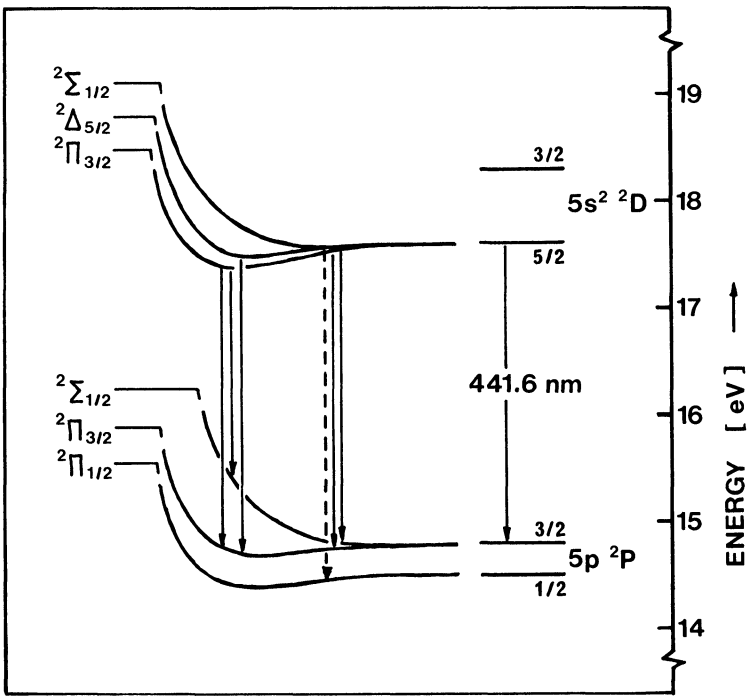

Figure 10 Relevant potential energy curves for the ionic He··Cd$^+$ complex. The spacing of the atomic energy levels is to scale; energies and shape of the potentials are only approximate in analogy to equivalent potential energy curves for He··Sr$^+$,Ca$^+$.[35,36] Possible molecular transition: → transitions between states correlating to the asymptotes of the atomic levels of the 441.6 nm line; - - - → other allowed molecular transitions.

able to generate wing emission slightly further away from the line centre. The bound to continuum transition $^2\Pi_{3/2} \rightarrow {}^2\Sigma^+_{1/2}$ will most likely give rise to a red wing extending far away from the line centre.

As discussed earlier and as can be seen in Figure 8 a strong blue wing is observed extending over 40 nm towards shorter wavelengths. This would indicate that the well depth of the lower (5pπ) $^2\Pi_{3/2}$ potential is at least 0.3 eV. As an alternative explanation for the wide blue wings the following argument could be followed. While the asymptotic transition $^2D_{5/2} \rightarrow {}^2P_{1/2}$ is forbidden ($\Delta J = 2$) the molecular $^2\Sigma^+_{1/2} \rightarrow {}^2\Pi_{1/2}$ transition is not; this transition therefore would be a shorter wavelength, providing approximately the required 0.3 eV. However, the transition between states with potential minima at very different interatomic separation may not generate the required band shape. The transition $^2\Pi_{3/2} \rightarrow {}^2\Pi_{1/2}$ which would be between states of similar shape, and which would also provide a blue shift, is forbidden in Hund's case *a* representation.

It should be stressed that the arguments followed here are plausible when one accepts the analogy of the Cd$^+$ – He pair to other metal (ion)—rare gas complexes; by no means need such analogy be correct. Further experimental investigation is necessary to provide data sets from which potential energy curves can be deduced employing standard procedures of line broadening.

6. CONCLUSION

In conclusion, the results of our detailed spectroscopic investigation of a multi-line hollow-cathode $HeCd^+$ laser has revealed how important it is to conduct such a study under lasing conditions. Other spectroscopic studies in non-lasing environments have been performed, for example using a simple single-anode single-hollow-cathode device[6] or a spark-produced plasma.[41] Both those studies concentrate on the dependence of lines of atomic neutral and ionic species to deduce information on energy transfer mechanisms. However, both fail to reveal contributions from molecular species in the discharge spectra. One reason for this may be the limited dynamic range of the detection system (most likely the case in[41]) which needs to be rather high to reveal the weak molecular bands stretching over a wide spectral range. Our experimental set-up has a dynamic range of up to $\simeq 32{,}000$ which provides sufficient signal-to-noise ratio to resolve the weak molecular features of He_2^* and Cd_2^*. Admittedly this capability of the system was only fully exploited with hindsight: once the laser emission lines had been identified as being extremely asymmetric which after elimination of system errors could only be attributed to broadening mechanisms, namely the formation of collision complexes, was a systematic search initiated to verify the molecular origin of some spectral features.

We can summarize the results of this spectroscopic study in three major points.

(i) The spectroscopic evidence of He_2^* and its pressure dependence, in relation to atomic He* emission, is a clear confirmation that at higher pressures He_2^+ becomes a major constituent of the laser discharge. This in turn explains part of the pressure dependence of the green $He\text{-}Cd^+$ laser lines thus filling a gap in the understanding of the related population mechanisms.

(ii) Broad emission bands originating from the Cd_2^* dimer have been observed; however, all indications are that Cd_2^*, other than He_2^+, does not play a major role in the lasing process.

(iii) Strong molecular bands accompany all laser lines, and the only plausible explanation is that they originate from the molecular complex $(He{\cdot\cdot}Cd^+)^*$. These spectra are most striking since all indications are, evaluating their intensity dependence on laser parameters, that the molecular transitions exhibit gain (this will be discussed in more detail in[17]). This is further confirmation that the spectroscopy of discharges of laser media should ideally be conducted while the laser is operating; otherwise important features may be missed and conclusions drawn in extrapolating to laser action may possibly be incorrect.

We have made all efforts to link the observed spectra to molecular states. However, at present there are only very few and insufficient theoretical data available for Cd_2 and none for $(He{\cdot\cdot}Cd^+)$ to allow us to make an assignment of spectral features to transitions between particular molecular states by simulation procedures. Thus far our experimental data sets are not sufficient to uniquely convert spectral intensity distributions to molecular potentials; measurements are now under way to provide the necessary data. Furthermore, attempts will be made to calculate theoretical potential energy curves for $(He{\cdot\cdot}Cd^+)$ using the pseudo-potential model approach in analogy to e.g., $(He{\cdot\cdot}Ca^+)$ and $(He{\cdot\cdot}Sr^+)$.

Acknowledgements

Part of this research was supported financially (grant S/CI1*-900821) by the Commission of the European Communities (CEC). S.E. Acosta-Ortiz would like to thank the CEC and CONACyT-Mexico for providing a research fellowship. Karyono gratefully acknowledges sponsorship through the Indonesian BPP Teknology Overseas Fellowship Programme.

References

1. G. R. Fowles and W. T. Silfvast, *IEEE J. Quantum Electron.* **QE-1**, 131 (1965).
2. K. Fujii, T. Takahashi and Y. Asami, *IEEE J. Quantum Electron.* **QE-11**, 111 (1975).
3. A. Fuke, K. Masuda and Y. Tokita, *Jap. J. Appl. Phys.* **27**, 602 (1988) and references therein.
4. P. Baltayan, J. C. Pebay-Peyroula and N. Sadeghi, *J. Phys. B: At. Mol. Phys.* **18**, 3615 (1985).
5. C. Grey Morgan, I. D. Hopkin and H. H. Telle, *Proc. S.P.I.E.* **701**, 171 (1987).
6. C. Boulmer-Leborgne, B. Dubreuil and J. C. Pellicer, *J. Phys. D: Appl. Phys.* **22**, 512 (1989).
7. C. E. Webb, in "High Power Gas Lasers", *Inst. Phys. Conf. Series.* **29**, 39 (1975) and references therein.
8. K. H. Wong and C. Grey Morgan, *J. Phys. D: Appl. Phys.* **16**, L1 (1983) and references therein.
9. I. D. Hopkin, Ph.D. thesis, University of Wales, Swansea (1987).
10. W. T. Silfvast, L. H. Szeto and O. R. Wood II, *Appl. Phys. Lett.* **39**, 212 (1981).
11. C. Boulmer-Leborgne, B. Dubreuil, B. Oumarou and J. C. Pellicer, *J. Phys. D: Appl. Phys.* **21**, 390 (1988).
12. M. Kamin and L. M. Chanin, *Appl. Phys. Lett.* **29**, 756 (1976).
13. C. B. Collins and W. W. Robertson, *J. Chem. Phys.* **40**, 2202 (1964) and *J. Chem. Phys.* **40**, 2208 (1964).
14. F. Ranjbar, H. H. Harris and J. J. Leventhal, *Appl. Phys. Lett.* **31**, 385 (1977).
15. H. H. Telle, I. D. Hopkin, P. Ramalingam and C. Grey Morgan, *J. Phys. D: Appl. Phys.* **21**, S167 (1988).
16. P. Ramalingam, Ph.D. thesis, University of Wales, Swansea (1989).
17. S. E. Acosta-Ortiz, Karyono and H. H. Telle, in preparation for publication.
18. J. A. Hornbeck and J. P. Molnar, *Phys. Rev.* **84**, 621 (1951).
19. J. S. Cohen, *Phys. Rev. A.* **13**, 86, 99 (1976).
20. G. Myers and A. J. Cunningham, *J. Chem. Phys.* **67**, 247 (1977) and *J. Chem. Phys.* **67**, 1942 (1977).
21. B. T. McClure, R. A. Johnson and R. B. Holt, *Phys. Rev.* **79**, 232 (1950).
22. R. K. Curran, *J. Chem. Phys.* **38**, 2974 (1963).
23. F. Emmert, H. H. Angermann, R. Dux and H. Langhoff, *J. Phys. D: Appl. Phys.* **21**, 667 (1988).
24. W. A. Rogers and M. A. Biondi, *Phys. Rev.* **134**, A1215 (1964).
25. Karyono, Ph.D. thesis, University of Wales, Swansea (1991).
26. N. Allard and J. Kielkopf, *Rev. Mod. Phys.* **54**, 1103 (1982) and references therein.
27. B. Wellegehausen and H. Welling, *Laser und Optoelectronik.* **16**, 105 (1984) and references therein.
28. V. E. Bondyby and J. H. English, *Chem. Phys. Lett.* **111**, (1984) and references therein.
29. J. Schlejen, Ph.D. thesis, University of Leiden, Holland (1987).
30. A. Kowalski, *Z. Naturforschung A.* **39**, 1134 (1984).
31. A. Kowalski, M. Czajkowski and W. H. Breckenridge, *Chem. Phys. Lett.* **119**, 368 (1985).
32. R. E. Drullinger and M. Stock, *J. Chem. Phys.* **68**, 5299 (1978).
33. C. F. Bender, T. N. Rescigno, H. F. Schäfer III and A. E. Orel, *J. Chem. Phys.* **71**, 1122 (1979).
34. F. H. Mies, W. J. Stevens and M. Krauss, *J. Mol. Spectrosc.* **72**, 303 (1978).
35. W. H. Breckenridge and H. Umemoto, in "Dynamics of Excited States", K. P. Lawley (ed.), (Wiley, New York, 1982), p. 325 and references therein.
36. N. Sato, S. Nambu and S. Iwata, *Chem. Phys. Lett.* **146**, 275 (1988).
37. T. Yamashita, *J. Chem. Phys.* **91**, 1451 (1989).
38. H. Harima, T. Ihara, Y. Urano and K. Tachibana, *Phys. Rev. A.* **34**, 2911 (1986).
39. T. S. Monteiro, I. L. Cooper, A. S. Dickinson and E. L. Lewis, *J. Phys. B: At. Mol. Phys.* **20**, 741 (1987).
40. J. Pascale, *Phys. Rev. A.* **28**, 632 (1983) and references therein.
41. A. Khare, V. Kumar and R. K. Thareja, *Z. Phys. D: At. Mol. Clust.* **6**, 67 (1987).